A&A 592, L2 (2016)
DOI: 10.1051/0004-6361/201628887

Astronomy & Astrophysics

Letter to the Editor

The southern hemisphere of 67P/Churyumov-Gerasimenko: Analysis of the preperihelion size-frequency distribution of boulders ≥7 m

Maurizio Pajola[1,2], Alice Lucchetti[3], Jean-Baptiste Vincent[4], Nilda Oklay[4], Mohamed R. El-Maarry[5], Ivano Bertini[2], Giampiero Naletto[2,6,7], Monica Lazzarin[8], Matteo Massironi[9], Holger Sierks[4], Cesare Barbieri[2,8], Philippe Lamy[10], Rafael Rodrigo[11,12], Detlef Koschny[13], Hans Rickman[14,15], Horst U. Keller[16], Jessica Agarwal[4], Michael F. A'Hearn[17], Maria A. Barucci[18,19], Jean-Loup Bertaux[20], Steve Boudreault[4], Gabriele Cremonese[3], Vania Da Deppo[7], Björn Davidsson[21], Stefano Debei[22], Mariolino De Cecco[23], Jakob Deller[4], Sonia Fornasier[18,19], Marco Fulle[24], Adeline Gicquel[4], Olivier Groussin[10], Pedro J. Gutierrez[25], Carsten Güttler[4], Marc Hofmann[4], Sebastian Höfner[4], Stubbe F. Hviid[26], Wing-Huen Ip[27], Laurent Jorda[10], Jörg Knollenberg[26], J.-Rainer Kramm[4], Ekkehard Kührt[26], Michael Küppers[28], Fiorangela La Forgia[8], Luisa M. Lara[25], Jui-Chi Lee[27], Zhong-Yi Lin[27], Jose J. Lopez Moreno[25], Francesco Marzari[8], Harald Michalik[29], Stefano Mottola[26], Frank Preusker[26], Frank Scholten[26], Nicholas Thomas[5], Imre Toth[30,10], and Cecilia Tubiana[4]

(Affiliations can be found after the references)

Received 10 May 2016 / Accepted 18 June 2016

ABSTRACT

Aims. We calculate the size-frequency distribution of the boulders on the southern hemisphere of comet 67P Churyumov-Gerasimenko (67P), which was in shadow before the end of April 2015. We compare the new results with those derived from the northern hemisphere and equatorial regions of 67P, highlighting the possible physical processes that lead to these boulder size distributions.

Methods. We used images acquired by the OSIRIS Narrow Angle Camera (NAC) on 2 May 2015 at a distance of 125 km from the nucleus. The scale of this dataset is 2.3 m/px; the high resolution of the images, coupled with the favorable observation phase angle of 62°, provided the possibility to unambiguously identify boulders ≥7 m on the surface of 67P and to manually extract them with the software ArcGIS. We derived the size-frequency distribution of the illuminated southern hemisphere.

Results. We found a power-law index of -3.6 ± 0.2 for the boulders on the southern hemisphere with a diameter range of 7–35 m. The power-law index is equal to the one previously found on northern and equatorial regions of 67P, suggesting that similar boulder formation processes occur in both hemispheres. The power-law index is related to gravitational events triggered by sublimation and/or thermal fracturing causing regressive erosion. In addition, the presence of a larger number of boulders per km^2 in the southern hemisphere, which is a factor of 3 higher with respect to the northern hemisphere, suggests that the southernmost terrains of 67P are affected by a stronger thermal fracturing and sublimating activity, hence possibly causing larger regressive erosion and gravitational events.

Key words. comets: general – comets: individual: 67P/Churyumov-Gerasimenko – methods: data analysis

1. Introduction

European Space Agency's (ESA) Rosetta spacecraft was inserted into orbit around the comet 67P/Churyumov-Gerasimenko in August 2014, providing a detailed surface characterization of the northern hemisphere thanks to the high resolution images acquired by the OSIRIS instrument (Optical, Spectroscopic, and Infrared Remote Imaging System; Keller et al. 2007). Since mid-May 2015, after the first nine months closely observing the 67P nucleus, the Rosetta spacecraft was moved into larger orbits around the comet. This was because 67P was getting closer to the Sun, leading to a greater surface activity and, hence, potential damages to the integrity of the spacecraft. Nevertheless, before performing wider excursions far from the target, Rosetta was sent closer to 67P in order to image its southern hemisphere and provide a morphological reference before perihelion. Indeed, by the end of April 2015, the southern terrains became fully illuminated by the Sun.

Detailed investigation regarding the different morphological features present on the northern hemisphere has been carried out (Sierks et al. 2015; Thomas et al. 2015; El-Maarry et al. 2015b; Vincent et al. 2015). In particular, by means of OSIRIS Narrow Angle Camera (NAC) images, analysis of cometary boulders, i.e., blocks that are ubiquitous on the surface of the comet, was performed for the first time (Pajola et al. 2015). Before the Rosetta arrival to 67P, multiple boulders analyses had been carried out on asteroidal surfaces, revealing that their origin is strictly related to impacts (Lee et al. 1986; Geissler et al. 1996; Thomas et al. 2001; Michikami et al. 2008; Küppers et al. 2012). For the cometary case, on the contrary, the impact-related origin has been discarded since there is only evidence on 67P for a single impact crater of 30 m (see Fig. 5b of El-Maarry et al. 2015a), and other formation processes like fragmentation, sublimation, outbursts, gravitational falls, and lifting processes were invoked to explain the formation of boulders (Pajola et al. 2015, 2016a).

The spatial distribution of boulders with a diameter ≥7 m has been reported on the overall northern hemisphere and equatorial regions of comet 67P, both on global and localized scales (Pajola et al. 2015). The analysis of the size-frequency distribution

Table 1. OSIRIS NAC dataset used in this work.

Day	UT	Distance (km)	Scale (m/px)
02-05-2015	04:54:10	125.4	2.32
02-05-2015	06:54:10	125.1	2.32
02-05-2015	07:54:10	125.1	2.32
02-05-2015	08:54:10	125.0	2.32
02-05-2015	10:42:52	124.9	2.31
02-05-2015	12:42:52	124.8	2.31
02-05-2015	15:09:42	124.9	2.31

Notes. All images were taken with the Orange filter F82, centered at 649.2 nm. The distance is from 67P center.

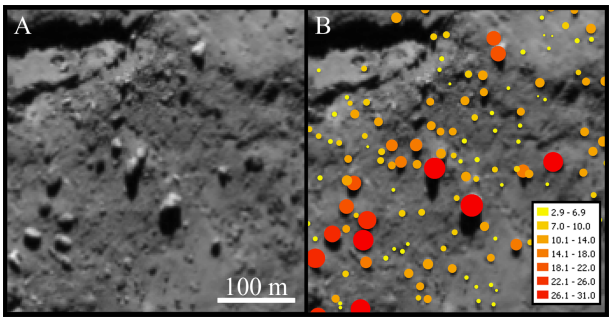

Fig. 1. Methodology used to identify the boulders on 67P. **A)** Subframe of a NAC image taken on 2 May 2015 at 06:54 UT. The scale of the image is 2.3 m/px. **B)** The detected boulders grouped in size (m).

(SFD), of boulders is a fundamental tool to interpret and understand the geomorphological context and the surface processes that occurred in various regions of the comet. For this reason, when high-resolution images of multiple areas of the comet were available, additional boulder counting has been performed, which has provided SFD in size ranges below 7 m; see, e.g., Vincent et al. (2015, 2016), Pommerol et al. (2015), Lucchetti et al. (2016), Pajola et al. (2016b), Oklay et al. (2016). Moreover, the results coming from such works proved that similar geomorphological settings display equivalent power-law indices even with different spatial scales (ranging from decameters to a minimum size of 1 m). Nevertheless, all previous results, as well as the different processes invoked to explain the formation and evolution of boulders (Pajola et al. 2015), refer only to the northern and equatorial regions of comet 67P. For this reason, by means of new images covering the previously hidden terrains, we obtained the SFD of boulders ≥7 m on the overall southern hemisphere with the main aim to complete the boulders analysis over the entire comet. In the following, after presenting the dataset and methods used in this work, we discuss the results obtained and we compare them with those found in the northern hemisphere. This is fundamental to understanding whether the boulders formation processes invoked for the northern hemisphere are valid for the southern hemisphere.

2. Dataset and methods

The southern hemisphere of comet 67P was illuminated at the end of April 2015, which is close to the comet's equinox (10 May, 2015) and before the insertion of Rosetta into larger orbits preceding perihelion (13 August, 2015). To complete the boulder identification, we started on the northern and equatorial regions of 67P and used the NAC images with the available highest spatial resolution (before perihelion) of the southern hemisphere ; these images were taken on 2 May 2015 at a distance of ~125 km and with a resulting scale of 2.3 m/px (see Table 1).

The nearly constant distance of the spacecraft from the comet surface (Table 1) provided a unique dataset where the resolution did not change over a full cometary rotation. This offered the possibility to derive meaningful statistics for boulders with diameters ≥7 m, i.e., the 3 pixels sampling that minimizes the likelihood of misidentifications of what we are detecting (Nyquist 1928). In addition, since the observations were performed with an almost constant phase angle[1] varying from 62° to 61°, the presence of elongated shadows on the surface allowed us to identify even smaller boulders (2 pixels diameter, ~4−5 m). As previously indicated in Pajola et al. (2015), however, we did not include these smaller populations in the binned cumulative SFD because they do not represent a complete dataset for such small sizes.

Before performing the boulder counting, we defined as "boulders"[2] the positive reliefs detectable in multiple images obtained with different observation geometries with the constant presence of an elongated shadow (if the phase angle is greater than 0°) whose extension depends on the illumination geometry (Pajola et al. 2015, 2016a). Moreover, we point out that a boulder seems to be detached from the ground where it stands.

Once such features were manually identified on the high-resolution images by using the ArcGIS software, we measured their position on the surface of the comet. We consequently assumed their shapes to be spherical[3], and we derived their maximum length, i.e., the diameter, and the corresponding area (Fig. 1). After that, we made use of the corresponding area computed from the three-dimensional (3D) shape model of 67P (Jorda et al. 2016) to obtain the binned cumulative boulder SFD per km^2.

3. Results

As for the case of the northern hemisphere of 67P and its equatorial regions, the boulders on the southern hemisphere are ubiquitous on the head, body, and neck (Thomas et al. 2015). The total number of boulders we identified is 4944, which lowers to 3503 when only the diameters ≥7 m are taken into account. Of the discarded 1441 smaller boulders, 820 fall in the 6−7 m bin, 335 are between 5 and 6 m, 238 between 4 and 5 m, and the remaining 48 are inside the 3−4 m bin. The spatial distribution of these boulders is presented in Fig. 2. The surface area of the southern hemisphere of the comet where we made our boulder counting is 12.0 km^2, which is equivalent to the ~25% of the total cometary surface (48.4 km^2, Jorda et al. 2016). By making use of such

[1] The constant phase angle is true for the body as a whole, but it varies on individual surfaces of the body, where facets are facing different directions. Nevertheless, the differently elongated shadows strongly helped in the boulder identification.

[2] We underline that this terminology is not meant to imply any structural similarity to the boulders normally seen on Earth, but when we identified a feature with the mentioned characteristics, we inferred that it was a boulder.

[3] To be consistent with Pajola et al. (2015), we focused on the maximum dimension of the circumscribed circle to each boulder. Nonetheless, this does not imply that the mechanisms we propose for boulders formation have to be equant. A morphometric shape distribution analysis of the boulders on higher resolution images, as performed, e.g., in Pajola et al. (2016a), Michikami et al. (2010), is not the scope of this work, but it is an ongoing activity we are accomplishing on 67P.

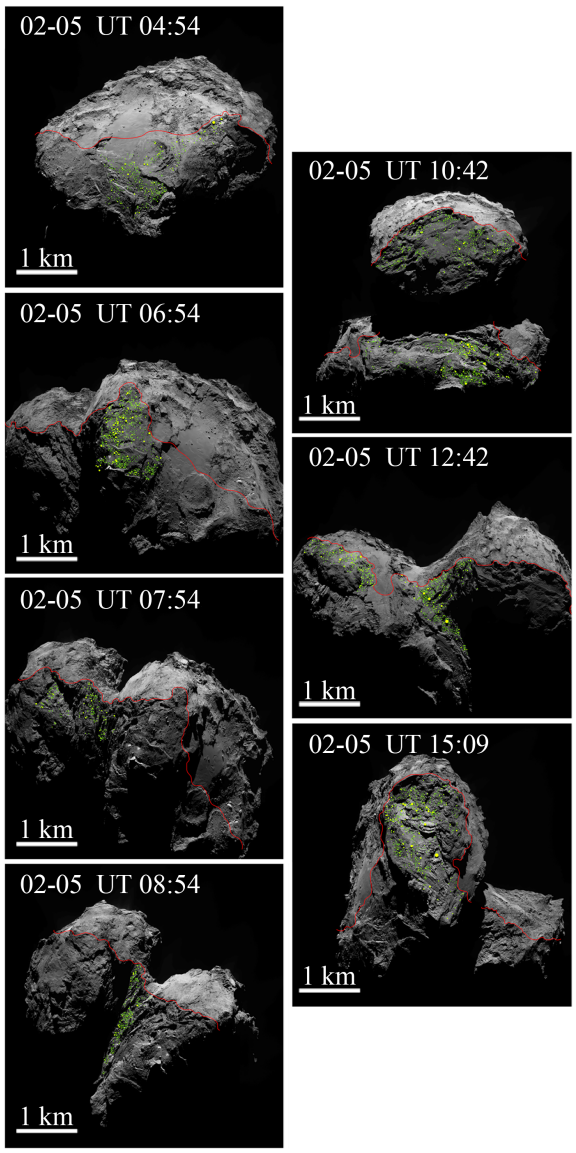

Fig. 2. Spatial distribution of the ≥7 m boulders on the southern hemisphere of 67P, derived from NAC images presented in Table 1. The red boundary shows the location of the terminator of the images presented in Fig. 8 of Pajola et al. (2015), i.e., the southernmost limit where the boulders where previously identified. We stress that, in each image, we only mapped those boulders that are located on areas mainly face-on with respect to the observer (we used the Jorda et al. 2016 shape model to assess this point). For this reason, we preferred to map them on one image and not on the previous or following images where they are still visible. Nonetheless, we used the entire dataset to double check the identification consistency, but counted the boulders only once in the final statistics.

value, we derived a binned cumulative number of 292 boulders ≥7 m per km^2. By fitting a regression line to the binned data[4], we

[4] The regression line used to detect the power-law index fits the binned values that are in the range of 7−35 m, but does not take into account those points that are equally cumulatively repeated. Indeed, as in Michikami et al. (2008), when subsequent values present the same cumulative number, this is an indication of a poor statistics that has does not have to be considered by the fit. This typically occurs at the bigger boulder sizes, i.e., for the case of Fig. 3A, above 35 m. Moreover, we point out that to correctly fit a cumulative distribution is not an obvious task, since the variables sizes and corresponding cumulative values are not independent (Lamy et al. 2004).

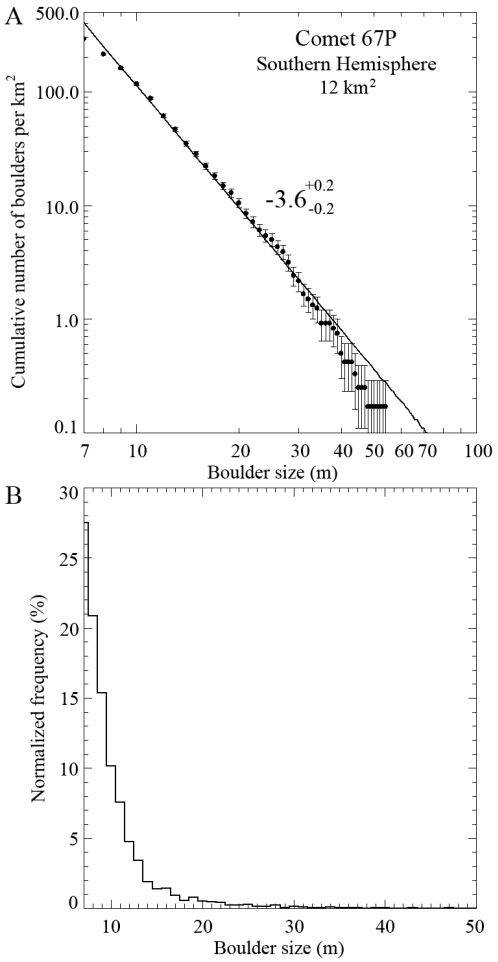

Fig. 3. A) Cumulative SFD of boulders ≥7 m per km^2 over the southern surface of 67P. Vertical error bars indicate the root of the cumulative number of counting boulders, divided by the area computed from the 3D shape model of 67P. The continuous line is a fitted regression line to the data, and the power-law index of the SFD is -3.6 ± 0.2. The bin size is 1 m. **B)** Histogram presenting the normalized frequency in percentage per boulder size. As above, the bin here is 1 m.

derived a value of -3.6 ± 0.2, that is the power-law index of the binned cumulative SFD of boulders ≥7 m per km^2; see Fig. 3A. In order to understand what the total percentage is for each contributing bin of the boulder statistics, we present, in Fig. 3B, the histogram of the normalized frequency per boulder size.

4. Discussion

After deriving the power-law index from the boulders of the southern hemisphere, we can draw comparisons with the values identified in other regions of 67P. Indeed, Pajola et al. (2015) showed that in the northern and equatorial areas of the comet, the power-law index computed in the range 7−38 m is −3.6 +0.2/−0.3, which is notably equivalent to the power-lawindex we obtained. By means of both global and local analyses, it was suggested that this power-law index could be related to gravitational events triggered by sublimation and/or thermal fracturing causing regressive erosion at the cliffs. Moreover, it was indicated that both the northern head and body of 67P are globally dominated by boulders originating from gravitational

events[5]. Therefore, the equivalent power-law index we derived here, can be indicative that sublimation and/or thermal fracturing causing regressive erosion and consequent gravitational collapse is the dominant process for the boulder formation in the southern hemisphere as well. Nonetheless, there are some notable differences that we have to point out, when the boulder SFD of the southern hemisphere is compared with previous results. The area we considered, 12 km^2, which only corresponds to 25% of the entire surface of the comet, is covered by an absolute number of boulders ≥7 m, 3503, which is comparable to the number of boulders, 3546, derived in the remaining 75% of the comet surface[6]. Correspondingly, we found that the binned cumulative number of boulders ≥7 m per km^2 is three times larger than the number of boulders identified on the northern and equatorial areas of 67P, namely 292 versus 97.

As presented in El-Maarry et al. (2016), the southern hemisphere of 67P is characterized by a clear dichotomy with respect to the northern hemisphere. This is mainly because there is a lack of widespread dust coatings and smooth terrains. The southernmost terrains of the comet are more similar to the consolidated terrains of the northern side, and almost always free of dust deposits (see Fig. 2). The southern hemisphere of 67P experiences a stronger insolation input than the northern hemisphere (Keller et al. 2015), as it is heated during and near the 2015 perihelion passage of 67P (1.24 AU) for 10 months, i.e., from May 2015 (1.73 AU) to March 2016 (2.47 AU). During the short southern summer (10 months out of a 6.5 yr long orbit), the higher sublimation activity triggered by the closer vicinity to the Sun, results in a factor of 3 higher erosive rates (Keller et al. 2015) with a possible release of larger proportion of escaping particles from the surface, which prevents a dusty blanket redeposition. Therefore, the fractured and rough terrains that characterize this hemisphere of 67P may be a possible direct consequence of a higher insolation input of this hemisphere of the comet.

We suggest that the higher activity that affects such areas of the comet may be invoked to explain the obtained results. Indeed, the same power-law index between the two hemispheres highlights the fact that similar erosive processes, such as sublimation and thermal fracturing, occur in both hemispheres. Nonetheless, the factor of 3 difference in the binned cumulative number of boulders per km^2 of the southern hemisphere with respect to the northern hemisphere may be related to the different sublimation, thermal stresses, and fracturing intensities. This possibly means that a larger thermal fracturing implies a higher sublimation activity. The consequence of this is that gravitational events occur more frequently on the surface with a consequent greater production than the northern hemisphere. Such interpretation is supported by the fact that in the southernmost terrains the boulders are typically in close proximity, or below, the surrounding cliffs from which they may have detached (El-Maarry et al. 2015b).

5. Summary and conclusions

This paper focused on the SFD of boulders ≥7 m located on the southern hemisphere of comet 67P. This area of the comet was in shadow before the beginning of April 2015 and, since May 2016, it has entered darkness again. By using images of the OSIRIS NAC camera on board Rosetta, we were able to derive the power-law index (-3.6 ± 0.2) of the binned cumulative boulder SFD in the size range of 7−35 m. This value is equivalent to the one that we derived in the northern and equatorial regions of 67P with the same size range. We therefore suggest that the equal power-law index may be indicative that sublimation and/or thermal fracturing causing gravitational collapse and consequent regressive erosion is the dominant process in the boulder formation of the southern hemisphere too. Nonetheless, a factor of 3 more boulders present in the southern hemisphere per km^2, with respect to the northern hemisphere, possibly suggests the fact that the southern, more active hemisphere, is affected by a stronger thermal fracturing and sublimating activity during its brief-but-intense summer. We therefore propose that most boulders are formed by regressive erosion when cliffs collapse and recede, in a similar way as has been observed for the northern hemisphere. This process is enhanced in the south by larger thermal stresses and higher level of activity, which are both due to much stronger insolation.

Acknowledgements. We would like to thank the anonymous referee for constructive comments, suggestions, and corrections that led to an important improvement of the paper. OSIRIS was built by a consortium of the Max-Planck-Institut für Sonnensystemforschung, in Göttingen, Germany, CISAS-University of Padova, Italy, the Laboratoire d'Astrophysique de Marseille, France, the Instituto de Astrofísica de Andalucia, CSIC, Granada, Spain, the Research and Scientific Support Department of the European Space Agency, Noordwijk, The Netherlands, the Instituto Nacional de Tecnica Aeroespacial, Madrid, Spain, the Universidad Politechnica de Madrid, Spain, the Department of Physics and Astronomy of Uppsala University, Sweden, and the Institut für Datentechnik und Kommunikationsnetze der Technischen Universität Braunschweig, Germany. The support of the national funding agencies of Germany (DLR), Italy (ASI), France (CNES), Spain (MEC), Sweden (SNSB), and the ESA Technical Directorate is gratefully acknowledged. We thank the ESA teams at ESAC, ESOC and ESTEC for their work in support of the Rosetta mission. M. Pajola was supported for this research in part by an appointment to the NASA Postdoctoral Program at the Ames Research Center administered by Universities Space Research Association (USRA) through a contract with NASA.

References

El-Maarry, M. R., Thomas, N., Giacomini, L., et al. 2015a, A&A, 583, A26
El-Maarry, M. R., Thomas, N., Gracia-Berná, A., et al. 2015b, Geophys. Res. Lett., 42, 5170
El-Maarry, N., Thomas, T., Gracia-Berna, A., et al. 2016, A&A, accepted, DOI:10.1051/0004-6361/201628634
Geissler, P., Petit, J.-M., Durda, D. D., et al. 1996, Icarus, 120, 140
Jorda, L., Gaskell, R., Capanna, C., et al. 2016, Icarus, accepted
Keller, H. U., Barbieri, C., Lamy, P., et al. 2007, Space Sci. Rev., 128, 433
Keller, H. U., Mottola, S., Davidsson, B., et al. 2015, A&A, 583, A34
Küppers, M., Moissl, R., Vincent, J.-B., et al. 2012, Planet. Space Sci., 66, 71
Lamy, P. L., Toth, I., Fernandez, Y. R., & Weaver, H. A. 2004, The sizes, shapes, albedos, and colors of cometary nuclei, ed. G. W. Kronk, 223
Lee, S. W., Thomas, P., & Ververka, J. 1986, Icarus, 68, 77
Lucchetti, A., Cremonese, G., Jorda, L., et al. 2016, A&A, 585, L1
Michikami, T., Nakamura, A. M., Hirata, N., et al. 2008, Earth, Planets, and Space, 60, 13
Michikami, T., Nakamura, A. M., & Hirata, N. 2010, Icarus, 207, 277
Nyquist, H. 1928, Trans. Am. Inst. Elect. Eng., 47, 617
Oklay, N., Sunshine, J. M., Pajola, M., et al. 2016, MNRAS, submitted
Pajola, M., Vincent, J.-B., Güttler, C., et al. 2015, A&A, 583, A37
Pajola, M., Lucchetti, A., Bertini, I., et al. 2016a, A&A, 585, A85
Pajola, M., Oklay, N., La Forgia, F., et al. 2016b, A&A, in press, 10.1051/0004-6361/201527865
Pommerol, A., Thomas, N., El-Maarry, M. R., et al. 2015, A&A, 583, A25
Sierks, H., Barbieri, C., Lamy, P. L., et al. 2015, Science, submitted
Thomas, N., Sierks, H., Barbieri, C., et al. 2015, Science, submitted
Thomas, P. C., Veverka, J., Robinson, M. S., & Murchie, S. 2001, Nature, 413, 394

[5] Some localized areas of 67P could have been affected by other processes that present a completely different power-law index, such as pit formation and escape of high-pressure volatiles, or evolved surface material undergoing continuous sublimation. On the contrary, the impact related origin for 67P boulders is discarded because there is only evidence on 67P of a single impact crater of 30 m (El-Maarry et al. 2015a).
[6] The Pajola et al. (2015) analysis was performed on images with the same spatial resolution as the dataset used here (Table 1).

Vincent, J.-B., Bodewits, D., Besse, S., et al. 2015, Nature, 523, 63
Vincent, J. B., Oklay, N., Pajola, M., et al. 2016, A&A, 587, A14

[1] NASA Ames Research Center, Moffett Field, CA 94035, USA
e-mail: maurizio.pajola@nasa.gov
[2] Center of Studies and Activities for Space, CISAS, "G. Colombo", University of Padova, via Venezia 15, 35131 Padova, Italy
e-mail: maurizio.pajola@unipd.it;
e-mail: maurizio.pajola@gmail.com
[3] INAF Osservatorio Astronomico di Padova, Vic. Osservatorio 5, 35122 Padova, Italy
[4] Max-Planck-Institut für Sonnensystemforschung, Justus-von-Liebig-Weg, 3 37077 Göttingen, Germany
[5] Physikalisches Institut der Universität Bern, Sidlerstr. 5, 3012 Bern, Switzerland
[6] Department of Information Engineering, University of Padova, via Gradenigo 6/B, 35131 Padova, Italy
[7] CNR-IFN UOS Padova LUXOR, via Trasea 7, 35131 Padova, Italy
[8] Department of Physics and Astronomy "G. Galilei", University of Padova, Vic. Osservatorio 3, 35122 Padova, Italy
[9] Geosciences Department, University of Padova, via G. Gradenigo 6, 35131 Padova, Italy
[10] Aix-Marseille Université, CNRS LAM (Laboratoire d'Astrophysique de Marseille), UMR 7326, 13388 Marseille, France
[11] Centro de Astrobiologa, CSIC-INTA, 28850 Torrejon de Ardoz, Madrid, Spain
[12] International Space Science Institute, Hallerstrasse 6, 3012 Bern, Switzerland
[13] Scientific Support Office, European Space Research and Technology Centre/ESA, Keplerlaan 1, Postbus 299, 2201 AZ Noordwijk ZH, The Netherlands
[14] Department of Physics and Astronomy, Uppsala University, 75120 Uppsala, Sweden
[15] PAS Space Reserch Center, Bartycka 18A, 00716 Warszawa, Poland
[16] Institute for Geophysics and Extraterrestrial Physics, TU Braunschweig, 38106 Braunschweig, Germany
[17] Department for Astronomy, University of Maryland, College Park, MD 20742-2421, USA
[18] LESIA-Observatoire de Paris, CNRS, UPMC, Univ. Paris 06, Univ. Paris-Diderot, 5 place J. Janssen, 92195 Meudon Principal Cedex, France
[19] Univ. Paris Diderot, Sorbonne Paris Cité, 4 rue Elsa Morante, 75205 Paris Cedex 13, France
[20] LATMOS, CNRS/UVSQ/IPSL, 11 boulevard d'Alembert, 78280 Guyancourt, France
[21] NASA Jet Propulsion Laboratory, 4800 Oak Grove Drive, Pasadena, CA 91109, USA
[22] Department of Mechanical Engineering, University of Padova, via Venezia 1, 35131 Padova, Italy
[23] UNITN, University of Trento, via Mesiano, 77, 38100 Trento, Italy
[24] INAF Osservatorio Astronomico di Trieste, via Tiepolo 11, 34143 Trieste, Italy
[25] Instituto de Astrofisica de Andalucia CSIC, Glorieta de la Astronomia, 18008 Granada, Spain
[26] Deutsches Zentrum für Luft- und Raumfahrt (DLR), Institut für Planetenforschung, Rutherfordstrasse 2, 12489 Berlin, Germany
[27] Institute for Space Science, National Central University, 32054 Chung-Li, Taiwan
[28] Operations Department European Space Astronomy Centre/ESA, P.O. Box 78, 28691 Villanueva de la Canada, Madrid, Spain
[29] Institut für Datentechnik und Kommunikationsnetze der TU Braunschweig, Hans-Sommer-Str. 66, 38106 Braunschweig, Germany
[30] Observatory of the Hungarian Academy of Sciences, PO Box 67, 1525 Budapest, Hungary